

Article

Preparation and Characterization of Apricot Kernel Shell Biochar and Its Adsorption Mechanism for Atrazine

Zhongqing Zhang¹, Chenhui Zhou², Jingmin Yang^{1,*}, Bingjian Yan², Jinhua Liu¹, Sinan Wang¹, Qi Li¹ and Mengmeng Zhou³

¹ Key Laboratory of Straw Comprehensive Utilization and Black Soil Conservation, Ministry of Education, College of Resource and Environmental Science, Jilin Agricultural University, Changchun 130118, China; zhangzhongqing@jlau.edu.cn (Z.Z.); liujinhua80@126.com (J.L.); a15114774751@163.com (S.W.); dqil822@163.com (Q.L.)

² Muyuan Foods Co., Ltd., Nanyang 473000, China; hqbgz@muyuanfoods.com (C.Z.); hqbz@muyuanfoods.com (B.Y.)

³ Jilin Anxin Food Technology Service Co., Ltd., Changchun 130012, China; zmmamember123@163.com

* Correspondence: yangjingmin@jlau.edu.cn; Tel.: +86-431-8453-3369

Abstract: In this study, the preparation of apricot kernel shell biochar by a hydrothermal method and its adsorption mechanism for atrazine was studied by scanning electron microscopy (SEM) and infrared spectrum (FTIR) analytical techniques. The results show that the biochar prepared from the apricot kernel shell has an evenly distributed, nonaggregated carbon microsphere structure and contains a large number of oxygen-containing groups. The higher the preparation temperature is, the more functional groups exist and the better the potential adsorption performance is. The adsorption kinetics of atrazine on apricot kernel shell biochar were fitted with a quasi-second-order kinetic equation ($R^2 \geq 0.995$, $p < 0.05$). The isothermal adsorption data were in accordance with the Freundlich model ($R^2 \geq 0.911$, $p < 0.05$). The adsorption of atrazine on apricot kernel shell biochar includes two processes: surface adsorption and diffusion. The adsorption capacity of apricot kernel shell biochar for atrazine increases with increasing preparation temperature and decreases with increasing pH and Ca^{2+} concentration. The adsorption mechanism includes hydrogen bonding and hydrophobic interactions. Therefore, biochar prepared from apricot shells, an agricultural waste, exhibits good adsorption performance for atrazine and has a good application prospect in addressing agricultural non-point source pollution, especially in pesticide residue pollution control.

Keywords: apricot shell; biochar; microspheres; atrazine; adsorption



Citation: Zhang, Z.; Zhou, C.; Yang, J.; Yan, B.; Liu, J.; Wang, S.; Li, Q.; Zhou, M. Preparation and Characterization of Apricot Kernel Shell Biochar and Its Adsorption Mechanism for Atrazine. *Sustainability* **2022**, *14*, 4082. <https://doi.org/10.3390/su14074082>

Academic Editors: Ram Swaroop Meena, Sandeep Kumar, Manoj Kumar Jhariya and Arnab Banerjee

Received: 2 March 2022

Accepted: 28 March 2022

Published: 30 March 2022

Publisher's Note: MDPI stays neutral with regard to jurisdictional claims in published maps and institutional affiliations.



Copyright: © 2022 by the authors. Licensee MDPI, Basel, Switzerland. This article is an open access article distributed under the terms and conditions of the Creative Commons Attribution (CC BY) license (<https://creativecommons.org/licenses/by/4.0/>).

1. Introduction

In recent years, the use of pesticides in agricultural production has increased crop yields, but overuse has also brought many environmental problems, such as soil contamination and other agricultural non-point source contamination problems [1]. Pesticides undergo a series of migration and transformation processes in the environment and generate new metabolites. The metabolites are more toxic and persist for a longer time than the pesticides themselves and are considered a new class of pollutants [2,3]. Atrazine is a highly effective herbicide with selective uptake and transmission before and after seedling growth and is suitable for controlling gramineous weeds, broad-leaved weeds and perennial weeds [4]. Atrazine has the characteristics of a stable structure, a long half-life (8–52 weeks) and difficult degradation. It can exist in water for a long time and has an impact on aquatic organisms and the human body [5]. The main degradation products of atrazine are de-ethyl atrazine, de-isopropyl atrazine and hydroxyatrazine, and the first two have similar toxicity to atrazine [6]. Therefore, scholars have performed extensive research on the environmental behaviour of atrazine and its pollution control, adsorption and degradation [7–10]. There are different degrees of atrazine pollution in natural water

worldwide. At present, the reported methods of removal include advanced oxidation, adsorption and photocatalytic degradation [11–13]. Pelekani et al. [14] used phenolic resin activated carbon to adsorb atrazine. Temperature and adsorption time have a great influence on the adsorption of atrazine. Ying et al. [15] used graphene oxide-loaded corn straw biochar to adsorb atrazine, and the removal amount of atrazine was 67.55 mg/g. Cao et al. [16] used sugarcane leaves, cassava stalks, rice straw and silkworm excrement to prepare biochar for atrazine adsorption. The higher the pyrolysis temperature was, the greater the adsorption capacity was.

In view of the simple use method and low price, biochar was widely used to solve the problem of organic contamination [17]. Biochar is a highly aromatic, insoluble and porous solid material produced by the pyrolysis and carbonization of biomass under low-oxygen or no-oxygen conditions. The main elements are C, H, O and S, and the content of C is more than 60%. Biochar has a multistage pore structure, a large specific surface area, a large number of surface negative charges and a high charge density. Furthermore, biochar is highly aromatic and highly stable, and its surface contains carboxyl, phenolic hydroxyl, carbonyl, lactone, pyranone, anhydride and other functional groups [18]. The existence of surface functional groups endows biochar with good adsorption performance [19]. The main biochar preparation methods are pyrolysis and hydrothermal carbonization. The pyrolysis method involves programmed temperatures of 200–800 °C, which are held for a certain time [20]. Pyrolysis biochar prepared by the pyrolysis method contains a certain amount of ash, but ash has no adsorption capacity. Hydrothermal carbonization biochar is prepared by applying a constant temperature of 180–250 °C, a pressure of 2–10 MPa and oxygen-free conditions with water as the medium in a special closed container for a certain time [21]. Hydrothermal carbonization biochar is characterized by simplicity, low energy consumption and environmental friendliness. Through dehydration and decarboxylation reactions, cellulose, hemicellulose and lignin in biomass are dehydrated and coked to form the unique carbon microsphere structure of hydrothermal carbon, which has a multistage pore structure, large specific surface area and high stability [22]. Xiang et al. [23] used rice straw to prepare hydrothermal carbonization biochar and pyrocarbon, and the adsorption capacity of methylene blue was 51.51 mg/g and 57.38 mg/g, respectively. Liu et al. [24] studied the adsorption of perfluorooctane sulfonate by *Camellia oleifera* seed shell hydrothermal carbon and found that after low-temperature hydrothermal treatment of *Camellia oleifera* seed shells, carbon microspheres were generated on the surface of the material, which was conducive to the adsorption of pollutants. Zhang et al. [25] found that pecan and peanut shell hydrothermal carbonization biochar had good adsorption performance for volatile organic compounds (VOCs). Yang et al. [26] used cotton and straw to prepare biochar at high temperatures to repair soil and adsorb chlorpyrifos and fipronil, processes that can reduce soil pollution and plant absorption. Li et al. [27] prepared walnut shell biochar to remove methylene blue and malachite green from water. The results showed that walnut shell biochar requires a low dosage as an adsorbent, is not easily affected by pH and has good adsorption performance. Therefore, agricultural waste has strong potential for the preparation of biochar to adsorb atrazine.

Apricot shell is a common waste in food production and processing. There are many pores on the surface and interior of apricot shells, which have a wood structure and are an excellent porous biomass material; apricot shells are often discarded or incinerated as garbage. At present, most research focuses on the preparation technology and pore structure of walnut shell activated carbon, while research on the micromorphology, phases and pore structure of apricot shell activated carbon is rarely reported. Kang et al. [28] prepared walnut shell biochar by hydrothermal carbonization and nitric acid modification, in which hemicellulose was completely decomposed and cellulose was partially decomposed to produce oxygen-containing functional groups. The aromaticity, specific surface area and pore content of the biochar increased, but the polarity decreased.

In this study, apricot shell was used as a raw material to prepare biochar, and the adsorption behaviour of atrazine was studied. The adsorption capacity was evaluated

by kinetic and thermodynamic models, and the adsorption mechanism was revealed. The results provide a theoretical basis for the preparation of apricot shell biochar and its adsorption performance for atrazine, as well as a reference for its application in remediating agricultural non-point source pollution.

2. Materials and Methods

2.1. Test Materials

Apricot shell was collected from Taonan City (E 123.19924, N 45.84779), Jilin Province; an atrazine standard (99.9%) was purchased from the National Standard Material Center; methanol (chromatographic purity), HNO₃, NaOH and CaCl₂ were all of analytical purity and purchased from Sinopharm; the test water was deionized water.

2.2. Preparation and Characterization of Biochar from Apricot Shell

2.2.1. Preparation of Hydrothermal Carbon Microspheres

The apricot shells were dried at 35 °C, crushed and passed through a 70-mesh sieve. A total of 3 g apricot shell powder was weighed, and 60 mL of deionized water was added. The mixture was stirred at room temperature for 30 min, transferred to the reactor, put in the electrically heated constant temperature drying oven and heated for 24 h at 190 °C, 200 °C, 210 °C, 220 °C or 230 °C. The sample was cooled to room temperature, removed, washed with deionized water until neutral and then dried for 8 h at 60 °C. The resulting biochar were denoted as XH-190, XH-200, XH-210, XH-220, XH-230 and XH-240, respectively.

2.2.2. Characterization of Biochar

The apparent morphology of the biochar prepared at different temperatures was measured and analysed by scanning electron microscopy (SEM; Tecnai G2F30, FEI, Hillsboro, OR, USA); infrared spectral analysis of the biochar prepared at different temperatures was carried out by using a Fourier transform infrared (FTIR) spectrometer (FTS6000, Bio-Rad Company, Hercules, CA, USA). Element analysis of the apricot kernel shell biochar was carried out by means of an element analyser (Vario El III, Hanau, Germany). The specific surface area and pore size distribution of the spherical apricot kernel shell biochar were measured by a static nitrogen adsorption instrument (3 h-2000ps1, Best Instrument Technology (Beijing) Co., Ltd., Beijing, China).

2.3. Adsorption of Atrazine by Biochar

2.3.1. Determination of Atrazine Adsorption Kinetics

The atrazine stock solution was diluted to the required concentration. A certain amount of apricot shell biochar (XH-190, XH-210 and XH-240) was put in a polyethylene centrifuge tube. Then, 9.5 mL of atrazine electrolyte solution with a concentration of 10 mg/L was added. The adsorption background solution was a 0.01 mol/L CaCl₂ solution (pH = 7). The tube was covered, sealed and placed on a constant temperature oscillator at 25 °C and 200 rpm in the dark for 24 h. Samples were taken at 10, 30, 60, 120, 300, 600, 900, 1440, 2160 and 2880 min. After centrifugation at 5000 rpm for 5 min, 2.5 mL supernatant was filtered through a 0.22 µm membrane and the concentration of atrazine in the solution was determined by high-performance liquid chromatography (HPLC). Chromatographic column: Gemini C¹⁸ (150 × 4.6 mm, 5 µm); column temperature: 30 °C; injection volume: 20 µL; mobile phase: methanol/water = 60/40 (v/v); flow rate: 1.0 mL/min.

2.3.2. Evaluation of Adsorption Thermodynamics

A total of 0.01 g biochar (XH-190, XH-210 and XH-240) was weighed into a 50 mL polyethylene centrifuge tube and 9.5 mL background solution (0.01 mol/L CaCl₂ atrazine solution) was added; the concentration gradient was 0, 5, 10, 15, 20, 30, 40 and 50 mg/L. Parallel experiments and blank controls were conducted for the above treatments. The whole process was carried out in dark conditions to avoid the photodegradation of atrazine

in the oscillation process. The concentration of atrazine in the supernatant under the conditions of 15 °C, 25 °C and 35 °C (± 0.5 °C) was determined by HPLC.

2.4. Influence of Different Factors on Atrazine Adsorption Capacity

2.4.1. Effect of Solution pH on Atrazine Adsorption Capacity

Biochar (HX-240, 0.02 g) was put in a polyethylene centrifuge tube, and 0.01 mol/L CaCl_2 was used as the background solution. A total of 12 mL of 30 mg/L atrazine solution were added to the tube, and the pH value of the background solution was adjusted to 3.0, 5.0, 7.0, 9.0 or 11.0 with 0.01 mol/L HNO_3 and NaOH. The content of atrazine in the supernatant was determined at 25 °C [29].

2.4.2. Effect of Ionic Strength on Atrazine Adsorption Capacity

A total of 0.02 g carbon (HX-240) was weighed into a polyethylene centrifuge tube, 12 mL of 30 mg/L atrazine solution was added and the initial concentration of CaCl_2 in the background solution was adjusted to 0.01, 0.05, 0.10, 0.15 or 0.20 mol/L. The content of atrazine in the supernatant was determined at 25 °C.

2.5. Data Processing

Origin 2019 software was used to draw the figures. SPSS 20.0 software was used to analyse the significance of experimental data ($p < 0.05$).

(1) Calculation of adsorption capacity

The amount of atrazine adsorbed by the biochar was calculated according to the following formula:

$$Q_e = \frac{(C_0 - C_e)V}{m} \quad (1)$$

where Q_e is the adsorption amount of atrazine (mg/g); C_0 and C_e are the initial concentration and equilibrium concentration of atrazine (mg/L); V is the volume of (adsorption) liquid; m is the mass of the adsorbent (g).

(2) Adsorption kinetic model

The adsorption kinetics of atrazine by the apricot shell biochar were fitted by using quasi-first-order and quasi-second-order dynamic models.

Quasi-first-order dynamic model:

$$\lg(q_e - q_t) = \lg q_e - k_1 t / 2.303 \quad (2)$$

Quasi-second-order dynamic model:

$$\frac{t}{q_t} = \frac{1}{k_2 q_e^2} + \frac{t}{q_e} \quad (3)$$

where q_e and q_t are the adsorption capacity of atrazine by biochar at time t and at equilibrium (mg/g); k_1 is the constant of the quasi-first-order adsorption model (/min); k_2 is the quasi-second-order adsorption model constant (g/mg/min).

The accuracy of the model (SSE %) was determined from the root mean square error, and the consistency between the calculated model and the experimental values is shown in Equation (4).

$$SSE\% = \sqrt{\frac{\sum (q_{e.exp} - q_{e.cal})^2}{N}} \cdot 100\% \quad (4)$$

where $q_{e.cal}$ and $q_{e.exp}$ are the calculated model values and experimental values (mg/g), respectively, and N is the number of experiments.

(3) Adsorption thermodynamics model

The Langmuir model and Freundlich model were used to fit the thermodynamic characteristics of atrazine adsorption by corn straw hydrothermal carbon.

Langmuir model:

$$Q_e = \frac{q_m K_L C_e}{1 + K_L C_e} \quad (5)$$

Freundlich model:

$$Q_e = K_F C_e^{1/n} \quad (6)$$

where Q_e is the adsorption capacity of the adsorbent (mg/g); q_m is the maximum single-layer adsorption capacity (mg/g); K_L is the Langmuir isotherm constant (L/mg); C_e is the equilibrium concentration (mg/g); n is a linear measurement of adsorption; K_F is the Freundlich isotherm constant.

According to the Langmuir model parameters, the standard Gibbs free energy (ΔG^θ), standard enthalpy change (ΔH^θ) and standard entropy change (ΔS^θ) were calculated by Equations (7) and (8).

$$\Delta G^\theta = \Delta H^\theta - T \Delta S^\theta \quad (7)$$

$$\Delta G^\theta = -R T \ln K \quad (8)$$

where ΔG^θ is the Gibbs free energy; R (8.314 J/K/mol) is the gas constant; T is the absolute temperature; K is the adsorption equilibrium constant of the Freundlich model; ΔH^θ is the change in enthalpy; ΔS^θ is the change in entropy. The values of ΔH^θ and ΔS^θ were calculated according to the slope and intercept of the plot of $\ln K$ vs. $1/T$.

(4) Contribution of diffusion and surface adsorption [30,31]

$$Q_T = Q_P + Q_A \quad (9)$$

$$Q_P = K_{oc} F_{oc} C_e \quad (10)$$

$$Q_A = K C_e^n - K_{oc} F_{oc} C_e \quad (11)$$

where Q_T is the total adsorption amount (mg/kg); Q_P is the atrazine adsorption amount caused by diffusion during the adsorption process; Q_A is the atrazine adsorption amount attributable to surface adsorption (mg/kg); K_{oc} is the distribution coefficient after normalization to the organic carbon content according to the K_d formula (L/kg); F_{oc} is the content of organic carbon in the tested material.

3. Results and Discussion

3.1. Characterization of Apricot Shell Biochar

3.1.1. Scanning Electron Microscopy (SEM) Images

The structure of the biochar was observed by SEM. Figure 1 shows that the structure of the apricot kernel shell biochar prepared at different temperatures is different. When the temperature is lower, the microspheres are more dispersed (A). With increasing temperature, the number of carbon microspheres increases (B), the surface area increases, the distribution becomes denser, and the size tends to be uniform (C). However, some carbon microspheres are bonded with each other. When the temperature is higher than 220 °C (D, E and F), the morphological structure of the biochar changes and some carbon particles become uniform. The microsphere structure is destroyed and a tubular structure appears.

3.1.2. Infrared Spectrum Characteristics

The surface functional groups were analysed by FTIR. Figure 2 shows that the apricot shell biochar prepared at different temperatures are rich in functional groups. The band at 3200–3640 cm^{-1} corresponds to the stretching vibration of O-H bonds in hydroxyl groups [32,33]. The antisymmetric stretching vibration of C-H bonds in methyl ($-\text{CH}_3$) groups is located at 2958 cm^{-1} , and the absorption peak of methylene in long-chain

saturated alkanes ($-\text{CH}_2-$) appears at $2838\text{--}2843\text{ cm}^{-1}$ [34,35]. The stretching vibration band of $-\text{CO-N}$ amide groups is located at $1690\text{--}1700\text{ cm}^{-1}$. The bands corresponding to carboxylic acid ($-\text{COOH}$) and carboxylic acid at $1540\text{--}1640\text{ cm}^{-1}$ indicate the existence of carbonyl groups ($-\text{C=O}$) and carboxylic acid, respectively [36]. The absorption peaks corresponding to the stretching vibration of aromatic carbonyl groups in lignin are located at 1600 cm^{-1} , 460 cm^{-1} and 450 cm^{-1} [37].

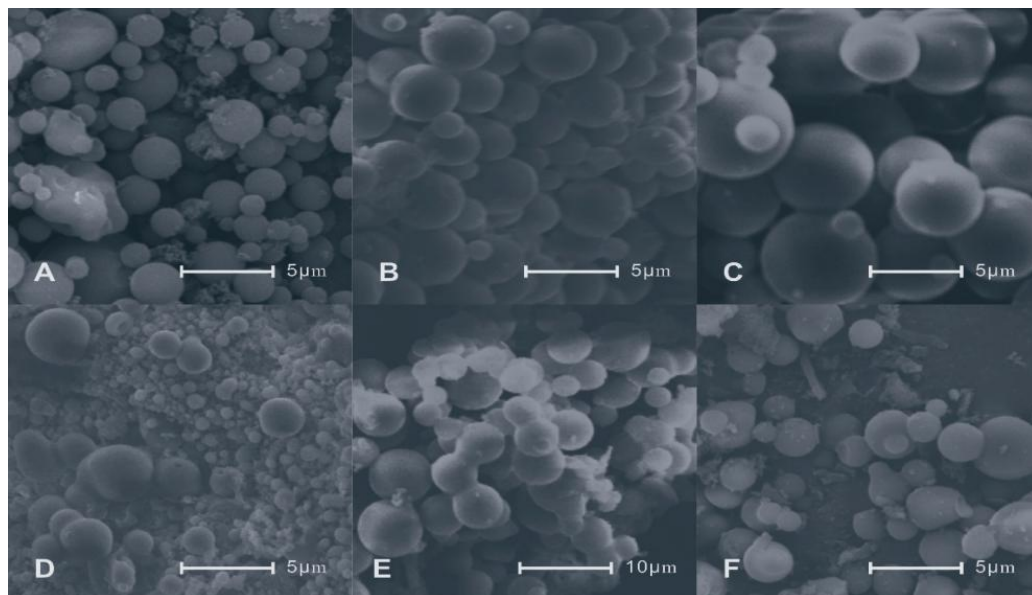


Figure 1. SEM images of apricot shell biochar. Note: (A–F) show the hydrothermal carbon micro-spheres prepared from apricot shells at 190, 200, 210, 220, 230 and 240 °C, respectively.

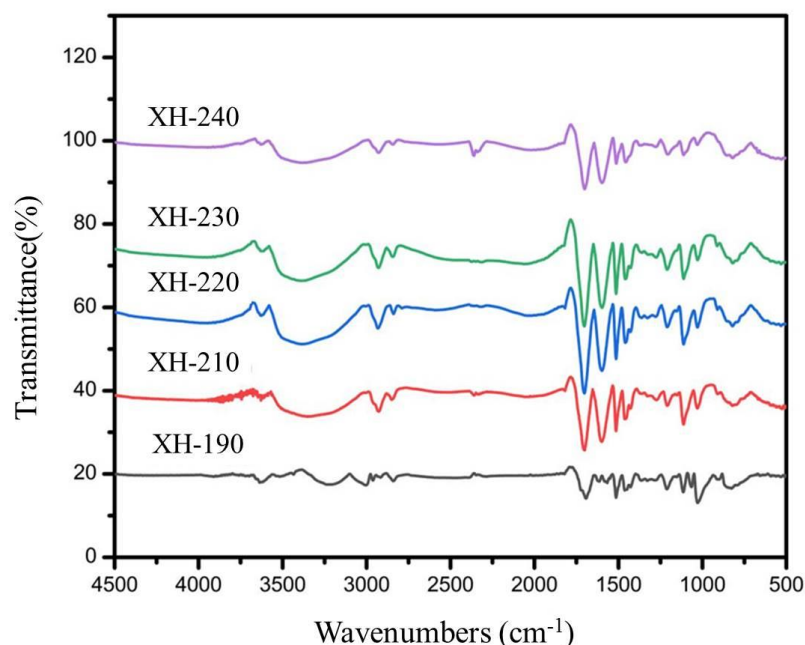


Figure 2. Infrared spectra of apricot kernel shell biochar.

3.1.3. Element Content of Apricot Shell Biochar

The elemental composition of the apricot kernel shell biochar was determined by an elemental analyser. Table 1 shows that with increasing carbonization temperature, the carbon content of the prepared biochar increases from 66.75% (190 °C) to 72.36% (240 °C); the hydrogen content decreases from 5.83% (190 °C) to 4.93% (240 °C); the nitrogen content

increases from 0.14% (190 °C) to 0.22% (240 °C). The loss of H and O in biochar is due to dehydration and decarboxylation [38]. The H/C and O/C ratios reflect the polarity of the biochar. H/C and O/C decrease with increasing temperature, indicating that the polarity of the biochar gradually decreases. The stronger the hydrophobicity of biochar is, the weaker the hydrophilicity, and the better the potential adsorption performance for organic pollutants.

Table 1. Element content of apricot shell biochar.

Sample	C (%)	H (%)	N (%)	C%/N%	(O + S) %	H/C (mol)	O/C (mol)	N/C (mol)
XH-190	66.75	5.83	0.14	452.91	27.32	1.16	0.33	0.0020
XH-200	67.66	5.61	0.16	431.98	26.56	1.00	0.29	0.0020
XH-210	69.99	5.14	0.18	382.40	24.69	0.88	0.26	0.0022
XH-220	69.06	5.22	0.18	388.16	25.54	0.91	0.28	0.0022
XH-230	70.71	5.36	0.21	333.23	23.71	0.91	0.25	0.0026
XH-240	72.36	4.93	0.22	322.63	22.48	0.82	0.23	0.0027

3.1.4. Analysis of Specific Surface Area and Pore Structure

The Brunauer–Emmett–Teller (BET) method was used to determine the specific surface area, pore volume and pore size of the biochar prepared at different temperatures. The results in Table 2 show that the specific surface area and average pore size of biochar prepared at different temperatures increase with increasing temperature, following the order XH-240 > XH-230 > XH-220 > XH-210 > XH-200 > XH-190. At 230 and 240 °C, the specific surface area and average pore size of biochar are almost the same, which indicates that there is a critical temperature in the process of biochar preparation. This finding is consistent with the conclusion of Nguyen and James et al. [39,40].

Table 2. Specific surface area and pore structure of apricot shell biochar.

Sample	Specific Surface Area (m ² /g)	Total Pore Volume (cm ³ /g)	Micropore Volume (cm ³ /g)	Average Aperture (nm)
XH-190	9.2873	0.0634	0.0058	0.8695
XH-200	9.3082	0.0598	0.0049	0.9073
XH-210	9.3112	0.0567	0.0042	0.9428
XH-220	9.3678	0.0492	0.0038	0.9839
XH-230	9.4149	0.0426	0.0036	1.0527
XH-240	9.4761	0.0391	0.0035	1.0669

3.2. Adsorption of Atrazine by Apricot Kernel Shell Biochar

3.2.1. Adsorption Kinetics

The adsorption kinetic curves of atrazine on the apricot kernel shell biochar are shown in Figure 3. The adsorption process is divided into two stages. The slope of the curve at the initial stage of adsorption (within 900 min) is larger, which indicates that the adsorption rate is fast, accounting for approximately 85% of the total amount of adsorption; the curve at the later stage of adsorption (900–2880 min) tends to be flat, and the adsorption rate is slow. In this experiment, adsorption equilibrium is reached at 2880 min. In this study, the first stage is the rapid adsorption stage, in which atrazine molecules quickly occupy the easily filled hydrophobic sites on the surface of biochar, so the adsorption capacity increases rapidly; the second stage is the slow adsorption stage, in which most of the easily filled hydrophobic sites on the surface of the adsorbent are occupied by atrazine and atrazine begins to occupy the pore structure of the biochar, resulting in a slow adsorption rate and a small decrease in adsorption capacity [41].

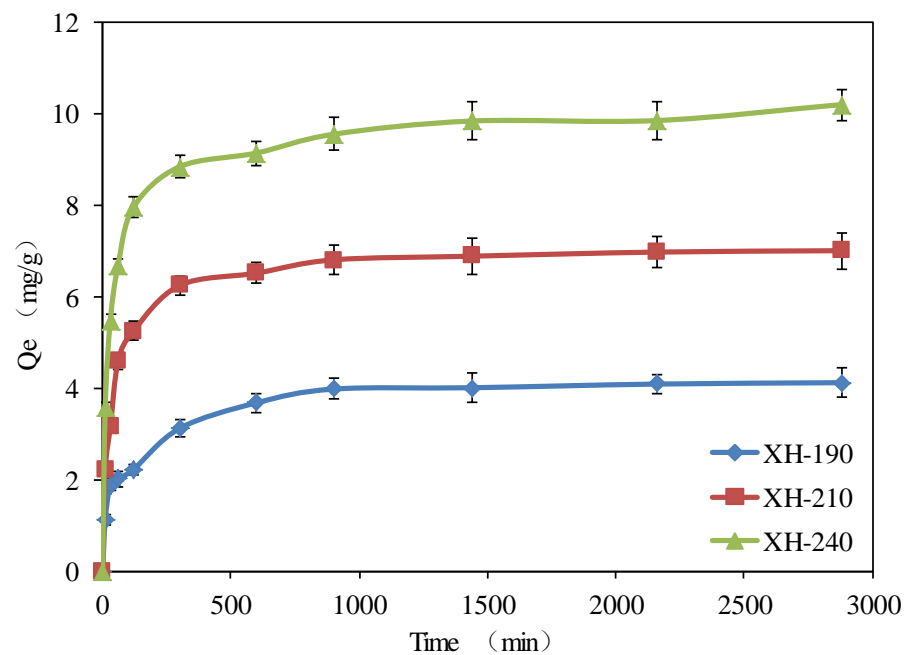


Figure 3. Kinetic curve of atrazine adsorption on apricot kernel shell biochar.

The adsorption kinetics of atrazine on apricot shell biochar were simulated by quasi-first-order and quasi-second-order models [42]. Table 3 shows that the fitting parameter (R^2) values for the adsorption of atrazine by apricot kernel shell hydrothermal carbon microspheres according to the quasi-first-order model are 0.906, 0.867 and 0.846, and the R^2 values for the quasi-second-order model are 0.995, 0.999 and 0.998. Therefore, the adsorption dynamics of atrazine on apricot kernel shell biochar are more consistent with the quasi-second-order model than the quasi-first-order model, indicating that the adsorption process is affected by various adsorption mechanisms, such as surface adsorption site transfer and external liquid film diffusion [43,44].

Table 3. Kinetic parameters of atrazine adsorption on apricot kernel shell biochar.

Sample	Quasi-First-Order			Quasi-Second-Order		
	Q_1 (mg/g)	K_1	r^2	Q_2 (mg/g)	K_2	r^2
XH-190	3.549	0.020	0.906	3.745	0.008	0.995
XH-210	6.077	0.026	0.867	6.355	0.006	0.999
XH-240	8.848	0.012	0.846	9.448	0.001	0.998

3.2.2. Adsorption Thermodynamics

The adsorption isotherms of atrazine on apricot kernel shell biochar are shown in Figure 4. With increasing ambient temperature, the adsorption capacity of atrazine on the biochar also increases because with increasing temperature, there are many oxygen-containing functional groups, such as -COOH, -CHO and -OH groups, on the surface of hydrothermal carbon [45]. These oxygen-containing functional groups cause the surface of the biochar to have a negative charge, and the negative charges form multiple exchange sites on the aromatic ring structure, which increases the cation exchange capacity of the biochar. An increase in temperature can increase the number of negative charges on the surface of biochar and then increase the adsorption capacity [46], indicating that the adsorption capacity of atrazine by apricot kernel shell biochar is affected by temperature. At the same temperature, the adsorption capacity of apricot kernel shell biochar prepared at three different temperatures for atrazine follows the order XH-240 > XH-210 > XH-190. This study shows that with increasing temperature, the larger the specific surface area and

average pore size of the biochar are, the more surface adsorption sites there are, and the better the adsorption performance is.

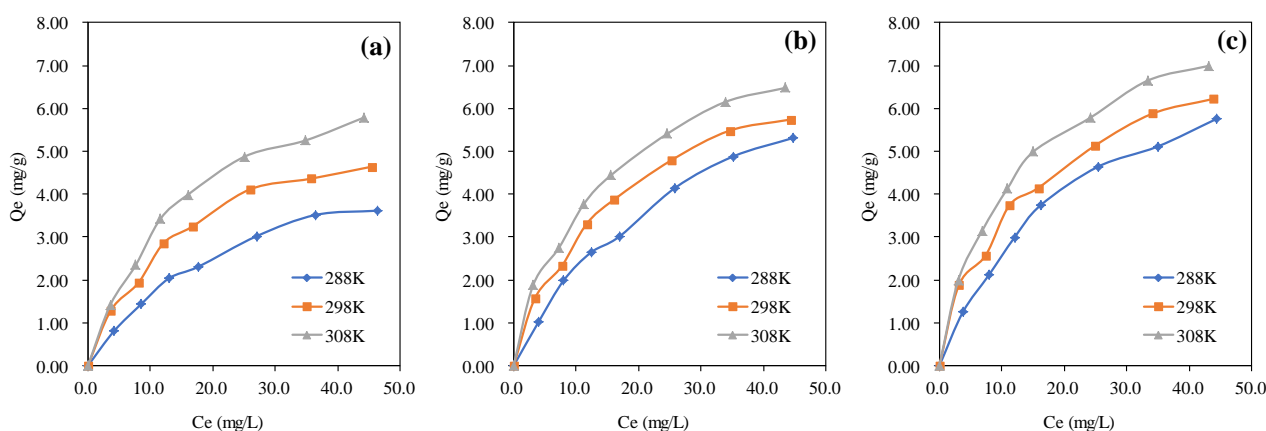


Figure 4. Adsorption isotherms of atrazine on apricot shell biochar. (a–c) show the biochar prepared from apricot shells at 190, 210, and 240 °C, respectively.

The Langmuir model, Freundlich model and Temkin model were used to fit the adsorption isotherms of atrazine on the apricot kernel shell biochar, as shown in Table 4. The Freundlich model fits the adsorption of atrazine on the apricot shell hydrothermal carbon microspheres well ($R^2 \geq 0.911$, $p < 0.05$), indicating that the adsorption belongs to multilayer heterogeneous adsorption [47,48]. In the Freundlich model, n is the nonlinear coefficient, and $n > 1$ indicates that the apricot kernel shell biochar exhibits nonlinear adsorption for atrazine. The Temkin model fitting results are also good ($R^2 \geq 0.965$, $p < 0.05$); this model mainly describes the chemical adsorption mechanism of electrostatic adsorption, indicating that the apricot kernel shell biochar also has electrostatic adsorption for atrazine.

Table 4. Isothermal adsorption parameters of atrazine on apricot kernel shell biochar.

Sample	Temperature (K)	Langmuir			Freundlich			Temkin		
		Q_m (mg/g)	k_L (L/mol)	r^2	n	k_F	r^2	a	b	r^2
XH-190	288	5.393	9736.2	0.945	2.019	246.1	0.911	15.706	1.418	0.952
	298	8.999	8382.1	0.979	1.643	186.2	0.964	21.015	1.836	0.965
	308	9.282	12,991.4	0.975	2.450	212.8	0.939	25.245	2.185	0.968
XH-210	288	8.179	8147.1	0.975	1.738	701.9	0.949	19.907	1.755	0.967
	298	11.259	10,316.1	0.978	1.854	783.7	0.950	28.279	2.445	0.968
	308	13.826	10,268.2	0.981	2.109	530.9	0.961	37.165	3.273	0.978
XH-240	288	11.732	12,843.2	0.984	2.343	322.9	0.959	32.603	2.83	0.982
	298	15.861	12,146.9	0.996	2.202	546.4	0.981	42.806	3.706	0.995
	308	18.931	13,538.8	0.986	2.382	492.2	0.953	51.741	4.449	0.981

The thermodynamic parameters calculated according to the Gibbs free energy are shown in Table 5. $\Delta G^\theta < 0$ and $\Delta H^\theta > 0$, which indicates that the adsorption of atrazine by apricot kernel shell biochar is a spontaneous endothermic reaction. The enthalpy and entropy of XH-190 adsorption are $\Delta H^\theta = 10.88$ kJ/mol and $\Delta S^\theta = 0.11$ kJ/mol, and the enthalpy and entropy of XH-210 adsorption are $\Delta H^\theta = 8.35$ kJ/mol and $\Delta S^\theta = 0.10$ kJ/mol, respectively. The adsorption enthalpy and entropy of XH-240 are $\Delta H^\theta = 2.014$ kJ/mol and $\Delta S^\theta = 0.09$ kJ/mol, and ΔH^θ is less than 40 kJ/mol. Therefore, the adsorption of atrazine on apricot kernel shell biochar is dominated by physical adsorption.

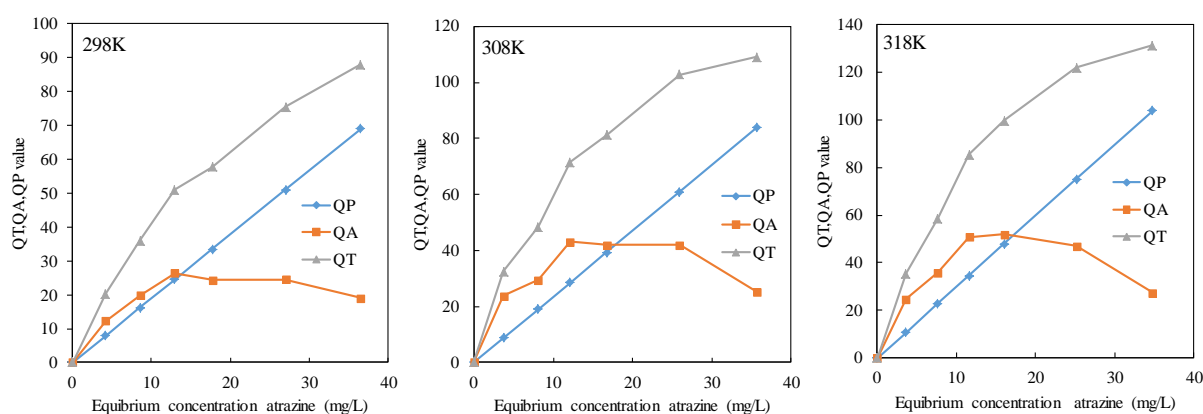
Table 5. Thermodynamic adsorption parameters of atrazine on apricot kernel shell biochar.

Sample	Temperature (K)	ΔG^θ (kJ/mol)	ΔS^θ (kJ/mol)	ΔH^θ (kJ/mol)
XH-190	288	−21.99	0.11	10.88
	298	−22.38		
	308	−24.26		
XH-210	288	−21.56	0.10	8.35
	298	−22.90		
	308	−23.65		
XH-240	288	−22.65	0.09	2.01
	298	−23.30		
	308	−24.05		

3.3. Contribution of Diffusion and Surface Adsorption to Atrazine Adsorption

Some nonlinear adsorption phenomena can be explained by a comprehensive adsorption mechanism including diffusion and surface adsorption [49,50]. To explore the adsorption mechanism of atrazine on apricot kernel shell biochar, the adsorption capacity of atrazine on the microspheres was expressed by Formula (4) to study whether surface adsorption or diffusion dominated in the adsorption process.

Because the Freundlich model fitting parameter $n > 1$ in this study, the adsorption of atrazine on apricot kernel shell biochar is nonlinear, so the comprehensive adsorption mechanism can better explain the adsorption behaviour of atrazine on apricot kernel shell biochar. The QT, QP and QA curves of atrazine on apricot kernel shell biochar with an equilibrium solution concentration CE are shown in Figure 5. The adsorption of atrazine on apricot kernel shell biochar includes two processes: surface adsorption and diffusion. When the equilibrium solution concentration is low, the adsorption of atrazine on apricot kernel shell biochar mainly involves surface adsorption. At a higher equilibrium solution concentration, the adsorption of atrazine on apricot kernel shell biochar mainly involves surface adsorption. Once surface adsorption reaches saturation, diffusion is the main adsorption mechanism of atrazine on apricot kernel shell biochar. With increasing temperature, the contribution of surface adsorption to atrazine adsorption of apricot kernel shell biochar increases.

**Figure 5.** Contribution of diffusion and surface adsorption to atrazine adsorption by biochar.

3.4. Influencing Factors of Adsorption

Figure 6a shows the adsorption capacity of atrazine on apricot kernel shell biochar prepared at different temperatures. With increasing preparation temperature, the adsorption capacity of the biochar gradually increases. The biochar prepared at 240 °C has abundant pores and a carbon microsphere structure (Figure 1), which is conducive to the adsorption

of atrazine. This finding is similar to the adsorption results for asparagus biochar prepared by Xu et al. [51].

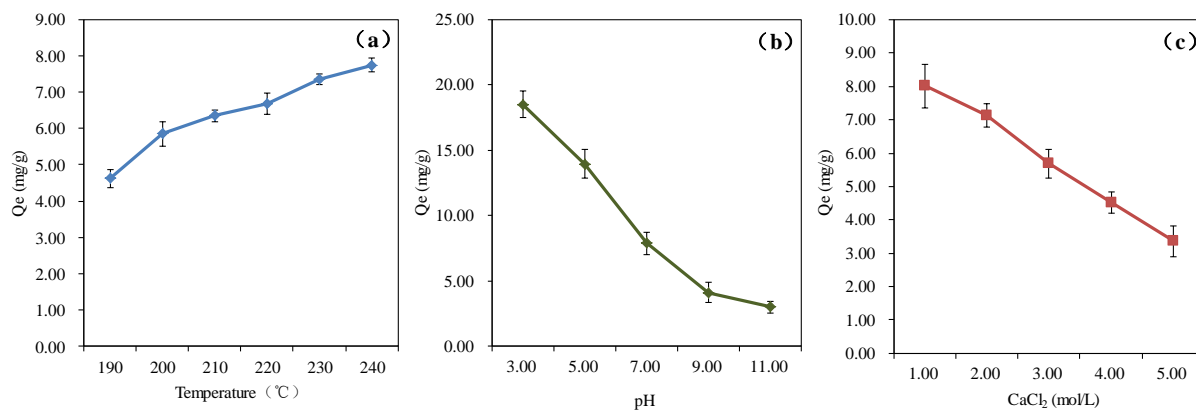


Figure 6. Effect of different factors on the adsorption of atrazine by biochar. (a–c) show the effect of temperature, pH and CaCl_2 , respectively.

Figure 6b shows the adsorption capacity of atrazine by biochar at different initial pH values. With increasing pH, the adsorption capacity decreases. When the pH value is greater than 9, the decrease in adsorption capacity decreases. With increasing pH, the dissociation reaction of atrazine occurs in water, resulting in the loss of protons and the hydrogen bond breaking of carboxyl groups, and organic matter polymers become anions with enhanced hydrophilicity. Therefore, the adsorption capacity of atrazine also decreases [52]. Li et al. [53] found that pH had a great influence on the adsorption of atrazine by sediments and that increased pH inhibited the adsorption of atrazine by sediments. Abate et al. [54] used modified montmorillonite to adsorb atrazine, and the adsorption capacity gradually decreased with increasing pH.

Figure 6c shows the adsorption capacity of biochar for atrazine in solutions with different ionic strengths. With increasing Ca^{2+} concentration in the solution, the adsorption capacity of biochar for atrazine decreases. The adsorption capacity of atrazine on hydrothermal carbon decreases from 7.720 mg/g to 3.451 mg/g. The adsorption of atrazine on biochar mainly involves cations [55]. When the content of Ca^{2+} in solution is too high, CaCl_2 will form and adsorb on the surface of biochar through electrostatic reaction, occupying the adsorption sites on the surface of biochar and thus reducing the adsorption capacity of the biochar for atrazine.

3.5. Adsorption Mechanism of Atrazine on Apricot Kernel Shell Biochar

Hydrothermal carbon is a highly aromatic, insoluble and porous solid material produced by the pyrolysis and carbonization of biomass under low-oxygen or no-oxygen conditions. The main elements are C, H, O and S, and the content of C is more than 60% [56]. Biochar has a multistage pore structure, a large specific surface area, a large number of surface negative charges and a high charge density. It is highly aromatic and stable. Its surface contains carboxyl, phenolic hydroxyl, carbonyl, lactone, pyranone, anhydride and other functional groups. The existence of surface functional groups endows hydrothermal carbon with good adsorption performance [57]. These functional groups are responsible for the complex interaction between apricot shell biochar and atrazine. Figure 7a,b show that the surface structure of the apricot kernel shell biochar before and after adsorption changes significantly. The surface structure of the carbon microspheres is destroyed, and the microspheres are deformed and bond to form a three-dimensional network porous structure, which indicates that there is a strong interaction between some functional groups of the apricot kernel shell biochar and atrazine. As seen from the infrared spectrum data in Figure 7c, O-H (3390 cm^{-1}) and C-O (1118 cm^{-1}) have the highest contents. The mechanism may include hydrogen bonding between the abundant carboxyl, phenolic

hydroxyl and carbonyl groups on the surface of the microspheres and nitrogen with lone pair of electrons on the surface of atrazine (Figure 7d). The triazine ring of atrazine is in face-to-face parallel contact with the aromatic rings on the surface of the microspheres, leading to the formation of atrazine. In addition, hydrogen bonding and hydrophobic interactions are the main adsorption forces. Therefore, hydrogen bonding and hydrophobic interactions may be the most important adsorption mechanisms of atrazine on apricot shell biochar. The absolute value of the free energy of atrazine adsorption on apricot kernel shell biochar is 21.56–24.26 kJ/mol, indicating that dipole–dipole interactions, electrostatic interactions and ion exchange are the secondary factors affecting atrazine adsorption on apricot kernel shell biochar.

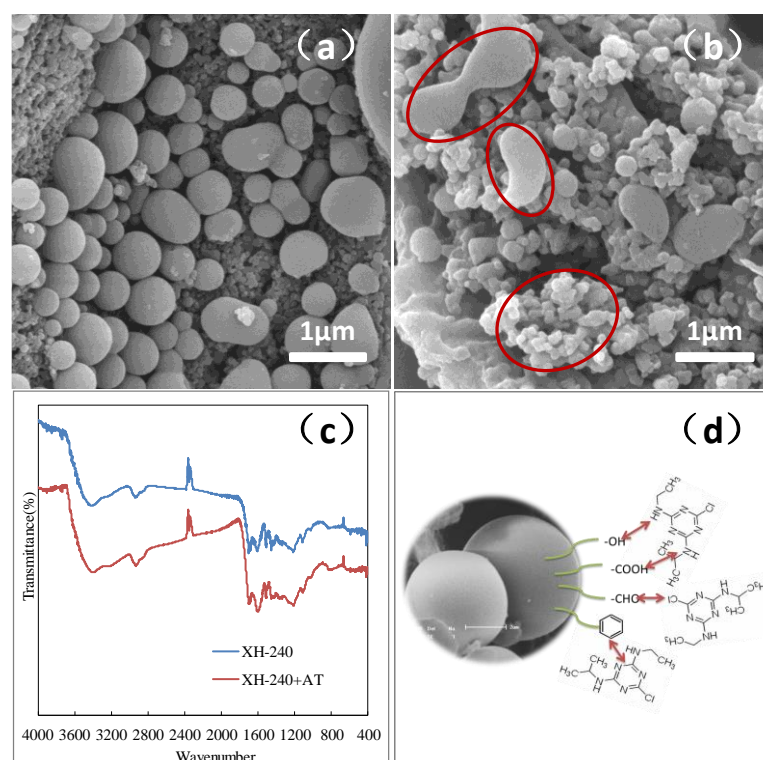


Figure 7. Adsorption mechanism of atrazine on biochar. (a,b) show the biochar SEM figure before and after adsorption changes; (c) show the biochar FTIR figure before and after adsorption changes; (d) show the adsorption mechanism.

4. Conclusions

With increasing carbonization temperature, the polarity of biochar decreases and the degree of organic matter cracking, aromaticity and hydrophobicity increases. The adsorption kinetics of atrazine on apricot kernel shell biochar are fitted by a quasi-second-order kinetic equation ($R^2 \geq 0.995$, $p < 0.05$). The isothermal adsorption data are in accordance with the Freundlich model ($R^2 \geq 0.911$, $p < 0.05$). The adsorption of atrazine on apricot kernel shell biochar includes surface adsorption and diffusion. With increasing temperature, the contribution of surface adsorption increases. The adsorption capacity of apricot kernel shell biochar for atrazine increases when the preparation temperature increases and decreases when the pH and Ca^{2+} concentration increase in the solution. The adsorption capacity of atrazine on biochar decreases from 7.720 mg/g to 3.451 mg/g. The adsorption mechanism of atrazine on apricot kernel shell biochar includes hydrogen bonding and hydrophobic interactions. Dipole–dipole interactions, electrostatic interactions and ion exchange are the secondary factors affecting the adsorption of atrazine on apricot kernel shell biochar.

Author Contributions: Z.Z. performed the experiments, collected the data and wrote the paper; J.Y. conceived and designed the experiments; J.L., S.W., Q.L. and M.Z. analysed the data; C.Z. and B.Y. contributed analysis tools and participate in part of the test experiments. All authors have read and agreed to the published version of the manuscript.

Funding: This work was supported by the Natural Science Foundation of Jilin Province (20210101367JC) and Horizontal issues of school enterprise cooperation (202020990).

Institutional Review Board Statement: Not applicable.

Informed Consent Statement: Not applicable.

Data Availability Statement: Not applicable.

Conflicts of Interest: All authors certify that they have no affiliations with or involvement in any organization or entity with any financial interest or non-financial interest in the subject matter or materials discussed in this manuscript.

References

1. Kankam, F. Causes and management of pesticides contamination in agriculture: A review. *Ghana J. Sci. Technol. Dev.* **2021**, *7*, 103–118. [[CrossRef](#)]
2. Richardson, S.D. Water analysis: Emerging contaminants and current issues. *Anal. Chem.* **2007**, *79*, 4295–4324. [[CrossRef](#)] [[PubMed](#)]
3. Ahmed, F.E. Analyses of pesticides and their metabolites in foods and drinks. *Trends Anal. Chem.* **2001**, *20*, 649–661. [[CrossRef](#)]
4. Solomon, K.R.; Giesy, J.P.; Lapoint, T.W.; Giddings, J.M.; Richards, R.P. Ecological risk assessment of atrazine in north american surface waters. *Environ. Toxicol. Chem.* **2013**, *32*, 10–11. [[CrossRef](#)]
5. Zhang, X.; Ma, X.; Li, X.; Li, C.; Wang, R.; Chen, M. Development of ultra-sensitive method for determination of trace atrazine herbicide in environmental water using magnetic graphene oxide-based solid-phase extraction coupled with dispersive liquid-liquid microextraction prior to gas chromatography-mass spe. *Water Air Soil Pollut.* **2018**, *229*, 1–11. [[CrossRef](#)]
6. Wang, L.R.; Zhao, M.Y. Study on the analysis method and influence of atrazine residues in irrigation water and soil. *J. Agro-Environ. Sci.* **2000**, *19*, 111–113. [[CrossRef](#)]
7. Ta, N.; Feng, J.F.; Sun, C.; Zhou, F. Determination of atrazine in Meiliang Bay of Taihu Lake by capillary gas chromatography. *Environ. Pollut. Control* **2005**, *8*, 634–636. [[CrossRef](#)]
8. Hoffman, R.S.; Capel, P.D.; Larson, S.J. Comparison of pesticides in eight U.S. urban streams. *Environ. Toxicol. Chem.* **2000**, *19*, 2249–2258. [[CrossRef](#)]
9. Buser, H.R. Atrazine and other s-triazine herbicides in lakes and in rain in Switzerland. *Environ. Sci. Technol.* **1990**, *24*, 1049–1058. [[CrossRef](#)]
10. Montiel-León, J.M.; Duy, S.V.; Munoz, G.; Bouchard, M.F.; Amyot, M.; Sauvé, S. Quality survey and spatiotemporal variations of atrazine and desethylatrazine in drinking water in Quebec, Canada. *Sci. Total Environ.* **2019**, *671*, 578–585. [[CrossRef](#)]
11. Zhang, P.; Sun, H.W.; Yu, L.; Sun, T.H. Adsorption and catalytic hydrolysis of carbaryl and atrazine on pig manure-derived biochars: Impact of structural properties of biochars. *J. Hazard. Mater.* **2013**, *244*, 217–224. [[CrossRef](#)] [[PubMed](#)]
12. Xu, L.; Zang, H.; Zhang, Q.; Chen, Y.; Wei, Y.; Yan, J.; Zhao, Y. Photocatalytic degradation of atrazine by H₃PW₁₂O₄₀/Ag-TiO₂. Kinetics, mechanism and degradation pathways. *Chem. Eng. J.* **2013**, *232*, 174–182. [[CrossRef](#)]
13. Khan, J.A.; He, X.; Khan, H.M.; Shah, N.S.; Dionysiou, D.D. Oxidative degradation of atrazine in aqueous solution by UV/H₂O₂/Fe²⁺, UV/S₂O₈²⁻/Fe²⁺ and UV/HSO₅⁻/Fe²⁺ processes: A comparative study. *Chem. Eng. J.* **2013**, *218*, 376–383. [[CrossRef](#)]
14. Pelekani, C.; Snoeyink, V.L. A kinetic and equilibrium study of competitive adsorption between atrazine and congo red dye on activated carbon: The importance of pore size distribution. *Carbon* **2001**, *39*, 25–37. [[CrossRef](#)]
15. Ying, Z.A.; Bo, C.A.; Lz, A.; Ls, A.; Yan, G.A.; JI, A.; Yang, F. Biochar-supported reduced graphene oxide composite for adsorption and coadsorption of atrazine and lead ions. *Appl. Surf. Sci.* **2017**, *427*, 147–155. [[CrossRef](#)]
16. Cao, M.Z.; Pan, L.P.; Zhang, C.L.; Yang, W.W.; Wei, J.M.; Zhang, F.L.; Wei, Y.H. Surface characteristics of four biomass carbons and their adsorption properties for cadmium-atrazine in aqueous solution. *J. Agric. Environ. Sci.* **2014**, *33*, 2350–2358. [[CrossRef](#)]
17. Ni, N.; Kong, D.; Wu, W.; Jian, H. The role of biochar in reducing the bioavailability and migration of persistent organic pollutants in soil–plant systems: A review. *Bull. Environ. Contam. Toxicol.* **2020**, *104*, 157–165. [[CrossRef](#)] [[PubMed](#)]
18. Jeyasubramanian, K.; Thangagiri, B.; Sakthivel, A.; Raja, J.D.; Rathika, B. A complete review on biochar: Production, property, multifaceted applications, interaction mechanism and computational approach. *Fuel* **2021**, *292*, 120243. [[CrossRef](#)]
19. Liang, B.; Lehmann, J.; Solomon, D. Black carbon increases cation exchange capacity in soils. *Soil Sci. Soc. Am. J.* **2006**, *70*, 1719–1730. [[CrossRef](#)]
20. Liu, D.D.; Li, J.M.; Zhao, B.J.; Zhu, J.H.; Chen, G.; Dong, L.J. Structure characterization and lead adsorption mechanism of straw hydrothermal carbon and pyrolysis carbon. *Trans. Chin. Soc. Agric. Mach.* **2020**, *51*, 304–314. [[CrossRef](#)]

21. Kalderi, D.; Kotti, M.S.; Méndez, A.; Gascó, G. Characterization of hydrochars produced by hydrothermal carbonization of rice husk. *Solid Earth* **2014**, *5*, 477–483. [[CrossRef](#)]
22. Shao, Y.C.; Lu, W.J.; Meng, Y. The formation of 5-hydroxymethylfurfural and hydrochar during the valorization of biomass using a microwave hydrothermal method. *Sci. Total Environ.* **2021**, *755*, 142499. [[CrossRef](#)] [[PubMed](#)]
23. Xiang, T.Y.; Shan, S.D.; Zhang, Z.H.; Lan, J.M. Characterization and adsorption characteristics of rice straw charcoal prepared by hydrothermal and thermal cracking. *Environ. Pollut. Control* **2019**, *41*, 75–79. [[CrossRef](#)]
24. Liu, Y.; Guo, H.Q.; Yan, L.S.; Lin, K.X.; Zeng, C.C.; Ma, W.T.; Bi, C.Y. Adsorption of perfluorooctane sulfonate (PFOS) in water by camellia seed shell carbon microspheres and their modified substances. *Environ. Chem.* **2016**, *35*, 2172–2182. [[CrossRef](#)]
25. Zhang, X.; Gao, B.; Fang, J.; Zou, W.; Dong, L.; Cao, C.; Zhang, J.; Li, Y.; Wang, H. Chemically activated hydrochar as an effective adsorbent for volatile organic compounds (VOCs). *Chemosphere* **2019**, *218*, 680–686. [[CrossRef](#)]
26. Yang, X.B.; Ying, G.G.; Peng, P.A.; Wang, L.; He, H.P. Influence of biochars on plant uptake and dissipation of two pesticides in an agricultural soil. *J. Agric. Food Chem.* **2010**, *58*, 7915–7921. [[CrossRef](#)]
27. Li, Y.; Shang, H.L.; Yuan, Z.W.; Fan, S.N.; Wang, N.; Liu, X.F.; Li, Z.X.; Tang, R.X. Adsorptive property of methy orange and malachite green onto walnut shell powder and walnut shell-derived biochar. *Guangzhou Chem. Ind.* **2018**, *46*, 48–50.
28. Kang, C.L.; Zhu, L.; Wang, Y.X.; Wang, Y.H.; Xiao, K.K.; Tian, T. Adsorption of basic dyes using walnut shell-based biochar produced by hydrothermal carbonization. *Chem. Res. Chin. Univ.* **2018**, *34*, 622–627. [[CrossRef](#)]
29. Zhou, M.M.; Zhang, Z.Z.; Zhao, Q.H.; Shao, W.Z.; Zhao, S.C.; Chang, H.B.; Yang, J.M. Preparation of hydrothermal carbon of cornstalks and its adsorption of atrazine in water. *J. Jilin Univ.* **2021**, *59*, 10. [[CrossRef](#)]
30. Zhu, L.; Chen, B. Sorption Behavior of p-Nitrophenol on the Interface between Anioncation Organobentonite and Water. *Environ. Sci. Technol.* **2000**, *34*, 2997–3002. [[CrossRef](#)]
31. Tian, X.H.; Xu, Y.J.; Zhang, X.Z.; Yu, Z.Q.; Zhang, H.W.; Deng, X.X.; Ren, C.B.; Zhang, L.M. Mechanism of semicarbazide adsorption on sediment of laizhou bay. *Environ. Pollut. Control.* **2013**, *35*, 50–52, 56. [[CrossRef](#)]
32. Weng, X.; Chen, Z.; Chen, Z.; Megharaj, M.; Naidu, R. Clay supported bimetallic Fe/Ni nanoparticles used for reductive degradation of amoxicillin in aqueous solution: Characterization and kinetics. *Colloids Surf. A Physicochem. Eng. Asp.* **2014**, *443*, 404–409. [[CrossRef](#)]
33. Fiorilli, S.; Rivoira, L.; Cali, G.; Appendini, M.; Bruzzoniti, M.C.; Coisson, M.; Onida, B. Iron oxide inside SBA-15 modified with amino groups as reusable adsorbent for highly efficient removal of glyphosate from water. *Appl. Surf. Sci.* **2017**, *411*, 457–465. [[CrossRef](#)]
34. Qiu, Y.; Ling, F. Role of surface functionality in the adsorption of anionic dyes on modified polymeric sorbents. *Chemosphere* **2006**, *64*, 963–971. [[CrossRef](#)] [[PubMed](#)]
35. Oezcimen, D.; Ersoy-Mericboyu, A. Characterization of biochar and bio-oil samples obtained from carbonization of various biomass materials. *Renew. Energy* **2010**, *35*, 1319–1324. [[CrossRef](#)]
36. Reza, M.T.; Lynam, J.G.; Uddin, M.H.; Coronella, C.J. Hydrothermal carbonization: Fate of inorganics. *Biomass Bioenergy* **2013**, *49*, 86–94. [[CrossRef](#)]
37. Malghani, S.; Gleixner, G.; Trumbore, S.E. Chars produced by slow pyrolysis and hydrothermal carbonization vary in carbon sequestration potential and greenhouse gases emissions. *Soil Biol. Biochem.* **2013**, *62*, 137–146. [[CrossRef](#)]
38. Baldock, J.A.; Smernik, R.J. Chemical composition and bioavailability of thermally altered *Pinus resinosa* (Red pine) wood. *Org. Geochem.* **2002**, *33*, 1093–1109. [[CrossRef](#)]
39. Nguyen, T.H.; Brown, R.A.; Ball, W.P. An evaluation of thermal resistance as a measure of black carbon content in diesel soot, wood char, and sediment. *Org. Geochem.* **2004**, *35*, 217–234. [[CrossRef](#)]
40. James, G.; Sabatini, D.A.; Chiou, C.T.; Rutherford, D.A.; Scott, C.; Karapanagioti, H.K. Evaluating phenanthrene sorption on various wood chars. *Water Res.* **2005**, *39*, 549–558. [[CrossRef](#)] [[PubMed](#)]
41. Henny, H.; Noort, P. Competition for adsorption between added phenanthrene and in situ PAHs in two sediments. *Chemosphere* **2003**, *53*, 1097–1103. [[CrossRef](#)]
42. Ying, G.G.; Kookana, R.S.; Dillon, P. Sorption and degradation of selected five endocrine disrupting chemicals in aquifer material. *Water Res.* **2003**, *37*, 3785–3791. [[CrossRef](#)]
43. Anyika, C.; Majid, Z.A.; Ibrahim, Z.; Zakaria, M.P.; Yahya, A. The impact of biochars on sorption and biodegradation of polycyclic aromatic hydrocarbons in soils—A review. *Environ. Sci. Pollut. Res.* **2015**, *22*, 3314–3341. [[CrossRef](#)] [[PubMed](#)]
44. Sun, Z.; Xu, J.; Wang, G.; Song, A.; Zheng, S. Hydrothermal fabrication of rectorite based biocomposite modified by chitosan derived carbon nanoparticles as efficient mycotoxins adsorbents. *Appl. Clay Sci.* **2019**, *184*, 105373. [[CrossRef](#)]
45. Yuan, J.H.; Xu, R.K.; Zhan, H. The forms of alkalis in the biochar produced from crop residues at different temperatures. *Bioresour. Technol.* **2011**, *102*, 3488–3497. [[CrossRef](#)]
46. Srivastava, V.; Weng, C.H.; Singh, V.K.; Sharma, Y.C. Adsorption of nickel ions from aqueous solutions by nano alumina: Kinetic, mass transfer, and equilibrium studies. *J. Chem. Eng. Data* **2011**, *56*, 1414–1422. [[CrossRef](#)]
47. Shu, Y.; Li, L.; Zhang, Q.; Wu, H. Equilibrium, kinetics and thermodynamic studies for sorption of chlorobenzenes on CTMAB modified bentonite and kaolinite. *J. Hazard. Mater.* **2010**, *173*, 47–53. [[CrossRef](#)]
48. Hameed, B.H.; Mahmoud, D.K.; Ahmad, A.L. Sorption equilibrium and kinetics of basic dye from aqueous solution using banana stalk waste. *J. Hazard. Mater.* **2008**, *158*, 499–506. [[CrossRef](#)]

49. Kasozi, G.N.; Zimmerman, A.R.; Nkedi-kizza, P.; Gao, B. Catechol and Humic acid sorption onto a range of laboratory-produced black carbons (biochars). *Environ. Sci. Technol.* **2010**, *44*, 6189–6195. [[CrossRef](#)]
50. Jonker, M.T.O.; Hawthorne, S.B.; Koelmans, A.A. Extremely slowly desorbing polycyclic aromatic hydrocarbons from soot and soot-like materials: Evidence by supercritical fluid extraction. *Environ. Sci. Technol.* **2005**, *39*, 7889–7895. [[CrossRef](#)]
51. Xu, Z.; Guo, Z.H.; Han, Z.Y.; Xiao, X.Y.; Sun, Y. Preparation of luzhu hydrothermal charcoal and study on separation mechanism of heavy metals. *Environ. Eng.* **2018**, *36*, 118–123. [[CrossRef](#)]
52. Yu, M.H. Study on the Adsorption and Desorption Effect and Mechanism of Atrazine in the Environment by Biochar. Ph.D. Thesis, China University of Mining and Technology, Beijing, China, 2014.
53. Li, Y.; Wang, Z.Z.; Wang, M.; Wang, Q. The effect of the interaction of various environmental factors on the adsorption of atrazine on sediments. *J. Jilin Univ.* **2013**, *1*, 334–339. [[CrossRef](#)]
54. Abate, G.; Masini, J.C. Adsorption of atrazine, hydroxyatrazine, deethylatrazine, and deisopropylatrazine onto Fe(III) polyhydroxy cations intercalated vermiculite and montmorillonite. *J. Agric. Food Chem.* **2005**, *53*, 1612–1619. [[CrossRef](#)] [[PubMed](#)]
55. Zhang, J.; Pang, R.; Duan, L.; Zhang, C.D. Study on the bioavailability of soil adsorbed atrazine. *Environ. Pollut. Control* **2013**, *35*, 12–16, 23.
56. Xiao, L.P.; Shi, Z.J.; Xu, F.; Sun, R.C. Hydrothermal carbonization of lignocellulosic biomass. *Bioresour. Technol.* **2012**, *118*, 619–623. [[CrossRef](#)] [[PubMed](#)]
57. Libra, J.A.; Ro, K.S.; Kammann, C.; Funke, A.; Berge, N.D.; Neubauer, Y.; Titirici, M.M.; Fühner, C.; Bens, O.; Kern, J. Hydrothermal carbonization of biomass residuals: A comparative review of the chemistry, processes and applications of wet and dry pyrolysis. *Biofuels* **2011**, *2*, 71–106. [[CrossRef](#)]